Ultrafast Interlayer Charge Transfer between Bilayer $PtSe_2$ and Monolayer WS_2

Pengzhi Wang,[†,‡] Dawei He,[‡] Yongsheng Wang,[*,‡] Xiaoxian Zhang,[‡] Xiaoyue He,[¶] Jiaqi He,[*,†] and Hui Zhao[*,§]

†*College of Mathematics and Physics, Beijing University of Chemical Technology, Beijing 100029, China*

‡*Key Laboratory of Luminescence and Optical Information, Ministry of Education, Institute of Optoelectronic Technology, Beijing Jiaotong University, Beijing 100044, China*

¶*Songshan Lake Materials Laboratory, Dongguan, Guangdong 523808, China*

§*Department of Physics and Astronomy, The University of Kansas, Lawrence, Kansas 66045, United States*

E-mail: yshwang@bjtu.edu.cn; jqhe@mail.buct.edu.cn; huizhao@ku.edu

Abstract

Interlayer charge transfer between $PtSe_2$ and WS_2 is studied experimentally. Layer-selective pump-probe and photoluminescence quenching measurements reveal ultrafast interlayer charge transfer in the heterostructure formed by bilayer $PtSe_2$ and monolayer WS_2, confirming its type-II band alignment. The charge transfer facilitates formation of the interlayer excitons with a lifetime of several hundred ps to 1 ns, a diffusion coefficient of 0.9 $cm^2\ s^{-1}$, and a diffusion length reaching 200 nm. These results demonstrate the integration of $PtSe_2$ with other materials in van der Waals heterostructures with novel charge transfer properties, and help develop fundamental understanding on the performance of various optoelectronic devices based on heterostructures involving $PtSe_2$.

KEYWORDS: $PtSe_2$, van der Waals heterostructure, charge transfer, interlayer exciton, transient absorption

Introduction

As a newly emerged two-dimensional (2D) material,[1–4] $PtSe_2$ nanofilms usually form a trigonal lattice.[5] Compared to the hexagonal transition metal dichalcogenides (TMDs), its band structures and electronic properties show stronger thickness dependence.[6,7] $PtSe_2$ changes from a zero-gap semimetal in bulk form[8] to a semiconductor with a 1.2-eV band gap in monolayers,[9,10] with semiconductor-to-semimetal transition occurring in the few-layer range.[11] Several techniques have been developed to fabricate 2D $PtSe_2$, including chemical vapor deposition (CVD),[12,13] molecular-beam epitaxy,[14] and selenization of 2D platinum films.[15] As many other 2D materials, monolayer and few-layer $PtSe_2$ can also be produced by simple mechanical exfoliation procedures.[16] The high-quality 2D $PtSe_2$ samples produced by these techniques allowed studies of their band structures,[9,17] charge transport properties,[18,19] and spin properties.[15,20] Potential applications of $PtSe_2$ in several types of devices have been investigated, such as field-effect transistors,[10] photovoltaic devices,[12] and photodetectors.[10,12,16,18,21]

Due to its novel electronic and optical properties, 2D $PtSe_2$ has been regarded as an attractive material to develop van der Waals heterostructures.[22] Very recently, such heterostructures have been fabricated and studied, combining 2D $PtSe_2$ with other layered materials, such as graphene,[17,23] MoS_2,[4,24] $MoSe_2$,[25] and PtS_2.[26] Interlayer charge transfer (CT) is an critical process to achieve superior electronic and optical properties of van der Waals heterostructures. For example, ultrafast charge transfer in several heterobilayers formed by TMDs has been observed.[27–33] However, charge transfer between $PtSe_2$ and other 2D materials has been less studied.

Here we report an experimental study on interlayer CT between bilayer $PtSe_2$ and monolayer WS_2. Photoluminescence quenching and transient absorption measurements reveal ultrafast CT processes, establishing a type-II band alignment of this structure. The lifetime and the diffusion coefficient of the interlayer excitons formed after CT are measured. These results establish $PtSe_2$ as a valuable member of the material library for developing 2D heterostructures with novel electronic and optoelectronic properties. The information revealed here is useful for developing fundamental understanding on the performance of $PtSe_2$-based devices.

Results and Discussion

The heterostructure sample of bilayer-$PtSe_2$/monolayer-WS_2 is schematically shown in Figure 1(a) and is obtained by stacking a mechanically exfoliated WS_2 monolayer flake onto a bilayer $PtSe_2$ film by dry transfer (see Experimental Section). Figure 1(b) shows an optical microscope image of the heterostructure sample. For comparison, another monolayer WS_2 flake is transferred onto the same substrate [Figure 1(c)]. The sample is thermally annealed at 473 K for 8 hrs in 2-Torr of Ar environment. This is a critical step, as previous studies have shown that thermal annealing enables a self-cleaning process utilizing the van der Waals force, with can significantly improve the interface quality.[34,35] To confirm the sample thickness, Figure 1(d) presents the Raman spectra of WS_2, $PtSe_2$, and heterostructure samples under 532-nm excitation. The two main peaks at 181 cm^{-1} and 209 cm^{-1} are assigned to the in-plane (E_g) and out-of-plane (A_{1g}) modes, respectively, according to previous reports.[10,12] The intensity ratio of the A_{1g} and E_g modes (0.26) confirms the bilayer thickness of the sample, according to the previously established result.[36] For WS_2, the two Raman modes observed at 356 and 417 cm^{-1} agree well with previously established results of monolayer WS_2.[37,38] From the heterostructure sample, features of both materials are observed.

We hypothesize the type of band alignment of this heterostructure based on the indi-

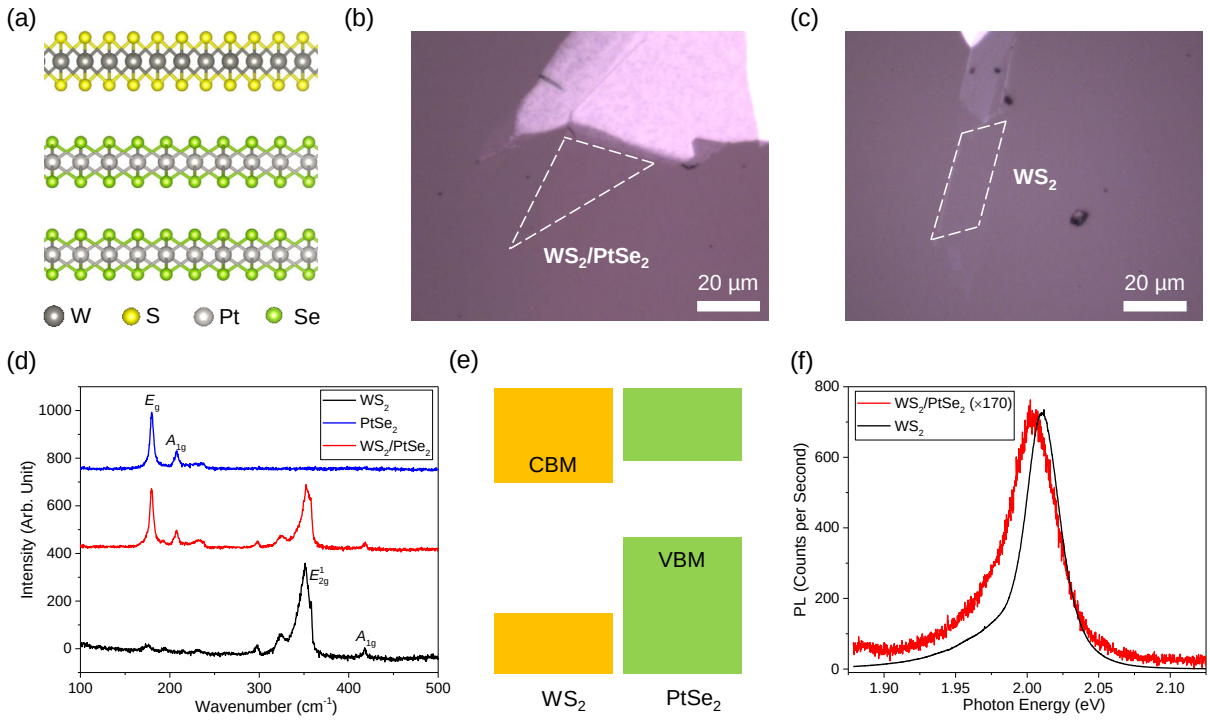

Figure 1: (a) Schematics of the crystalline structure of a heterostructure formed by monolayer WS_2 and bilayer $PtSe_2$. (b) and (c) Images of WS_2 monolayer on top of a bilayer $PtSe_2$ film and on a bare sapphire substrate, respectively. (d) Raman spectra of monolayer WS_2, bilayer $PtSe_2$, and their heterostructure samples. (e) Hypothesized type-II band alignment of the $WS_2/PtSe_2$ heterostructure. (f) Photoluminescence spectra of WS_2 monolayer and $WS_2/PtSe_2$ heterostructure (multiplied by 170).

vidual band structures of monolayer WS_2 and bilayer $PtSe_2$. Recent photoemission electron microscopy studies have determined the conduction band minimum (CBM) and valence band maximum (VBM) of monolayer WS_2 of -3.7 and -5.7 eV (measured from vacuum level), respectively.[39] Meanwhile, DFT calculations predicted typical CBM values in the range of -3.75 to -3.96 eV and VBM values ranging from -5.36 to -5.88 eV.[40–44] The relatively small range of the DFT results and their consistency with the experimental findings suggest that the band structure of monolayer WS_2 is well established. However, studies of band structure of bilayer $PtSe_2$ are rare, and with larger uncertainties. The band gap values of bilayer $PtSe_2$ predicted by DFT range from 0.21,[9,17] 0.35,[10] to as high as 1.0 eV.[45] An CBM of -4.51 eV and a VBM of -4.72 eV were predicted,[17] while the corresponding experimental values are -3.75 and -4.5 eV, respectively.[46] Based on these results, we can safely assume that the VBM

of bilayer $PtSe_2$ is within the forbidden band of monolayer WS_2. That is, it is higher than the VBM but lower than the CBM of monolayer WS_2. This rules out a type-III band alignment. However, the location of the CBM of bilayer $PtSe_2$ is rather uncertain. We hypothesize that it is higher than the CBM of monolayer WS_2, and thus the heterostructure forms a type-II band alignment, as shown in Figure 1(e). Our experimental results below will support this hypothesis.

To probe the interface quality and potential CT processes of the heterostructure, steady-state photoluminescence (PL) spectra of the heterostructure and monolayer WS_2, are measured under 2.33-eV and 1.3-μW excitation. As shown in Figure 1(f), a pronounced 2.01-eV peak is observed from WS_2, further confirming its monolayer thickness.[37,38] This peak is quenched by about 170 times in the heterostructure. Since the same WS_2 exciton density is excited in both samples, such significant PL quenching indicates that the WS_2 excitons in the heterostructure are much shorter lived than those in the individual WS_2 monolayer. This can be attributed to the additional decay channel provided by the $PtSe_2$ layer, *via* mechanisms of transfer of electrons or holes (*i.e.* CT) or transfer of both types of carriers (energy transfer). Previously, significant PL quenching has been established as a strong indicator of efficient interlayer CT or energy transfer.[47] The PL peak energy of the heterostructure is also lower than that of monolayer WS_2 by about 10 meV, which is due to the change of the band gap and exciton binding energy of WS_2 by the $PtSe_2$ layer through dielectric screening.[48,49]

Next, CT in the heterostructure is studied by transient absorption measurements using a homemade experimental setup, which details have been described previously.[32,33] A 3.02-eV and 1-μJ cm^{-2} pump pulse excites electrons (-) and holes (+) in both layers, as schematically shown in Figure 2(a). By using absorption coefficients[50,51] of 2×10^8 and 3.6×10^7 m^{-1} for WS_2 and $PtSe_2$, respectively, the pump pulse excites peak carrier densities of 3.2 and 1.1×10^{11} cm^{-2} in the WS_2 and $PtSe_2$ layers, accordingly. Based on the hypothesized type-II band alignment, electrons (holes) excited in $PtSe_2$ (WS_2) can transfer to WS_2 ($PtSe_2$). As shown (red arrow) in Figure 2(a), the probe pulse is tuned to the optical band gap of the WS_2

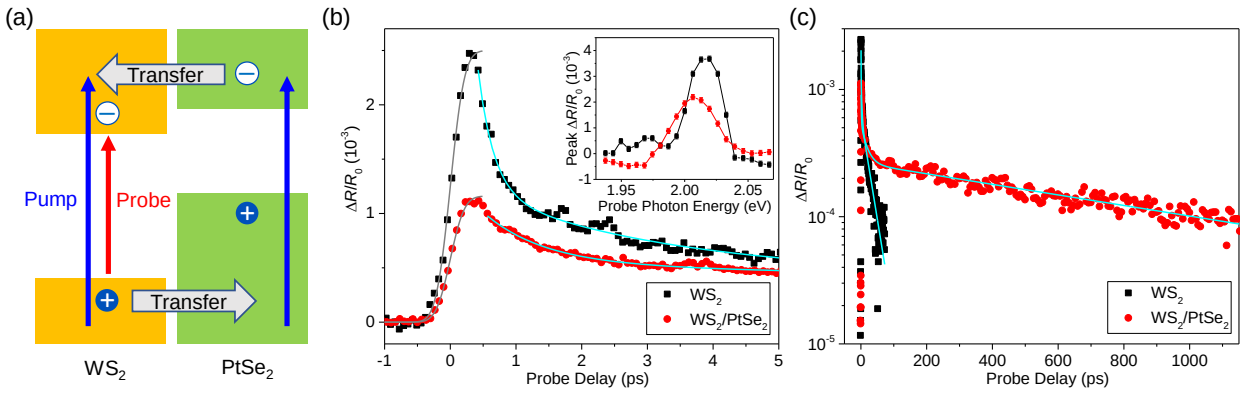

Figure 2: (a) Schematics of the pump-probe configuration where a pump pulse excites carriers in both layers of the $WS_2/PtSe_2$ heterostructure and a probe pulse senses carriers in WS_2. (b) Differential reflectance measured from the monolayer WS_2 (black) and the heterostructure (red). The curves are fits (see text). The inset shows the peak differential reflectance of the monolayer WS_2 (black) and the heterostructure (red) versus the probe photon energy. (c) Same as (b) but for a long time range. The curves are fits using an exponential decay function (see text).

monolayer and thus mainly senses its carrier population. This is achieved by measuring the percentage change of the probe reflectance by the pump excitation, known as differential reflectance, $\Delta R/R_0 = (R - R_0)/R_0$, where R and R_0 are the reflectance with and without the pump, respectively.[52] The result is shown in Figure 2(b) and 2(c) as the red circles, along with the result from the monolayer WS_2 sample (black squares) under the same conditions. The two signals are significantly different, with the former having a lower peak and a long-lived component that persists for over 1 ns. The observed difference confirms the existence of CT or energy transfer, which is consistent with the PL quenching shown in Figure 1(f). Without such transfer, the two signals would have been similar since both would reflect the photocarrier dynamics solely in the WS_2 layer. To further confirm that the probe pulse monitors the carriers in WS_2, the peak differential reflectance is measured as a function of the probe photon energy for each sample. Both signal show clear resonant features at the exciton resonance of WS_2 [Figure 2(b)].

To quantitatively analyses these results, we note that the signal from the WS_2 monolayer rises to a peak rapidly. We fit the signal with a Gaussian integral with a full width at half maximum of 0.4 ps, which is close to the cross-correlation of the two pulses, as shown by

the gray curve over the black squares in Figure 2(b). Such an instrument-limited rise time is consistent with previous pump-probe measurements of WS_2, and shows that the pump-injected carriers induces a peak differential reflectance on a time scale shorter than the time resolution of the measurement.[52] The decay of the WS_2 signal is fit by a triple exponential function, $\Delta R/R_0(t) = A_1\exp(-t/\tau_1) + A_2\exp(-t/\tau_2) + A_3\exp(-t/\tau_3)$, as shown by the cyan curve over the black squares in Figure 2(b) and 2(c), with three decay constants (and their weights) of 0.24 ± 0.03 ps (83 %), 2.4 ± 0.3 ps (9 %), and 27 ± 2 ps (8 %), respectively. The initial sub-ps fast decay have been previously assigned to the exciton formation process of the excited electron-hole pairs.[53–55] The 2.4- and 27-ps processes reflect the excitonic dynamics in monolayer WS_2, with the latter being the exciton recombination lifetime. These results agree well with previous studies.[52] The rise of the signal from the $WS_2/PtSe_2$ heterostructure sample is equally fast [Figure 2(b)]. Its decay is fit by the same exponential function, with three decay constants of 0.97 ± 0.1 ps (60 %), 18 ± 3 ps (20 %), and 1050 ± 50 ps (20 %), respectively.

We interpret the results from the heterostructure sample as the following: Upon injection, the holes excited in WS_2 transfer to $PtSe_2$ while the electrons excited in $PtSe_2$ transfer to WS_2, both occurring faster than 0.4 ps. Since the hole density injected in WS_2 is significantly higher than the electron density in $PtSe_2$, the electron and hole transfers result in a net loss of carrier density in WS_2 and thus a reduction of the peak signal. The transferred electrons and holes relax their energy and form interlayer excitons. These processes account for the 0.97-ps decay. The 1050-ps process is assigned to the long recombination lifetime of these interlayer excitons, due to the spatial separation of the electron and hole wavefunctions. It is also much longer than the exciton lifetime in bilayer $PtSe_2$, which is on the order of 100 ps, as will be shown below in Figure 4. Such long interlayer exciton lifetimes have been generally observed in type-II heterostructures.[28,47] The 18-ps process could be due to the dynamics of the excitons in WS_2 formed by electrons and holes that do not participate in the interlayer transfer process, due to low interface quality experienced by them.

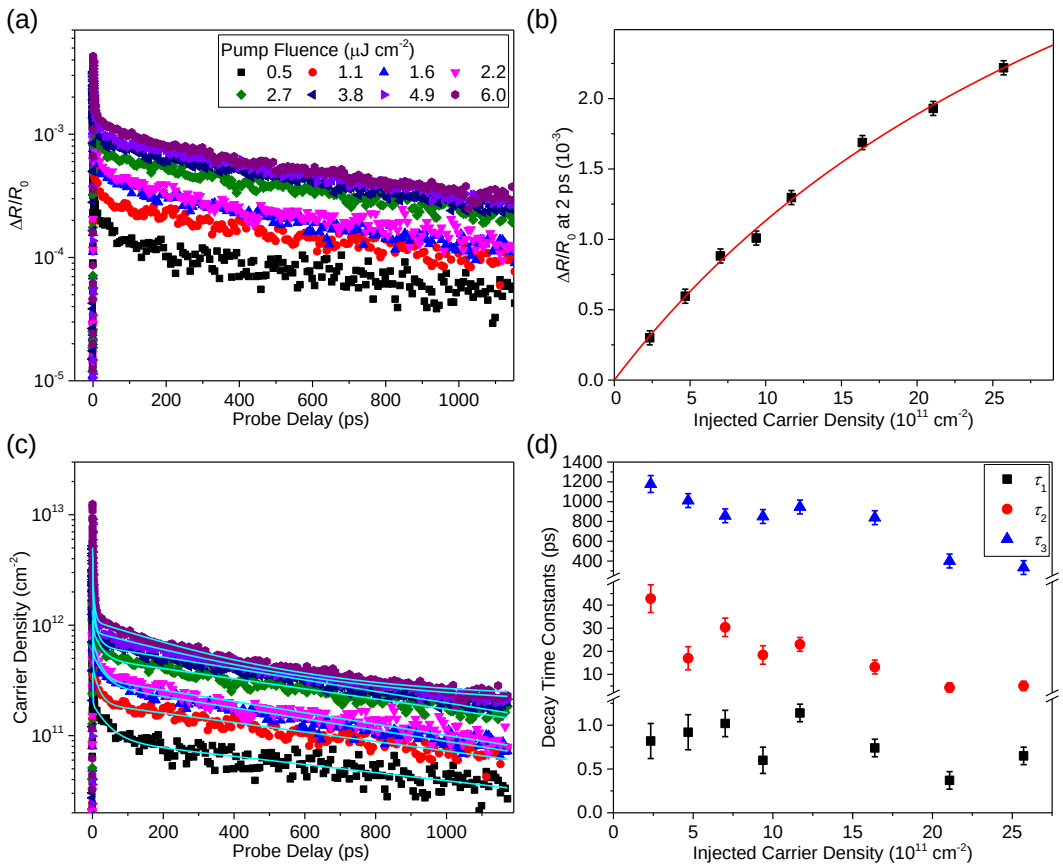

Figure 3: (a) Differential reflectance measured from the $WS_2/PtSe_2$ heterostructure using the configuration shown in Figure 2(a) but with various pump fluences. (b) Differential reflectance at a probe delay of 2 ps as a function of the pump-injected carrier density. (c) Time evolution of carrier density calculated from data shown in (a) by using the relation between the differential reflectance and the carrier density as shown in (b). (d) Time constants deduced from the exponential fits shown as the cyan curves in (c) as a function of the injected carrier density.

The nanosecond decay process observed in the heterostructure is strong evidence of its type-II band alignment as we hypothesized. If the alignment was type-I, both the CBM and VBM would be in $PtSe_2$, and thus electrons and holes excited in WS_2 should both transfer to $PtSe_2$. This additional channel should reduce the lifetime of carriers in WS_2, causing a faster decay of the signal compared to that of monolayer WS_2. Hence, the long-lived signal proves that one type of carriers (most likely electrons, based on our analysis on the band structures of both materials 6242) stay in WS_2 and are separated from their counterparts.

To further confirm the above interpretation, the measurement on the heterostructure

shown in Figure 2 is repeated with various pump fluences, as presented in Figure 3(a). To accurately relate the signal to the carrier density, the density-dependent differential reflectance at 2 ps is presented in Figure 3(b). Here, the injected carrier density is estimated from the pump fluence by using the aforementioned relation (that is, a 1-μJ cm^{-2} of the 3.02-eV pump pulse excites carrier densities of 3.2 and 1.1×10^{11} cm^{-2} in the WS_2 and $PtSe_2$ layers, respectively). The signal at 2 ps, instead of the peak signal, is used to avoid complications due to the exciton formation process. However, this choice does not impact our conclusion. The signal shows a nonlinear dependence on the injected carrier density, N, which can be well fit by an absorption saturation model,[56] $\Delta R/R_0 = AN/(N + N_s)$, as shown in Figure 3(b), with $A = 5.67 \times 10^{-3}$ and a saturation density $N_s = 4.0 \times 10^{12}$ cm^{-2}. Although transient absorption is typically proportional to the carrier density in the low-density regimes, such sub-linear dependence has been generally observed in 2D semiconductors at elevated densities, due to the saturation of the carrier-induced transient absorption at such densities.[52] This relation is then used to convert the differential reflectance shown in Figure 3(a) to the carrier density [in Figure 3(c)]. By fitting the carrier density by the aforementioned triple exponential function (cyan curves), we deduce the decay constants, as summarized in Figure 3(d). Both τ_2 and τ_3 decrease with increasing the carrier density, suggesting shorter intralayer and interlayer exciton lifetimes at higher densities. This feature is consistent with previously reported effects of exciton-exciton annihilation.[57,58] For comparison, the same power-dependent measurement is also performed on monolayer WS_2 (see Supporting Information Figure S1).

In the next configuration, we selectively excite electrons in $PtSe_2$ with a 1.51-eV pump and monitor their transfer to WS_2 by using a 2.01-eV probe, as schematically shown in Figure 4(a). With an absorption coefficient of 1×10^7 m^{-1},[51] the 16-μJ cm^{-2} pump pulse is estimated to inject carriers with a peak density of about 8×10^{11} cm^{-2} in $PtSe_2$. No excitation of the WS_2 layer is expected since the pump is below the its optical band gap. With the probe tuned to the exciton resonance of WS_2, it senses the electrons that are excited in $PtSe_2$ and

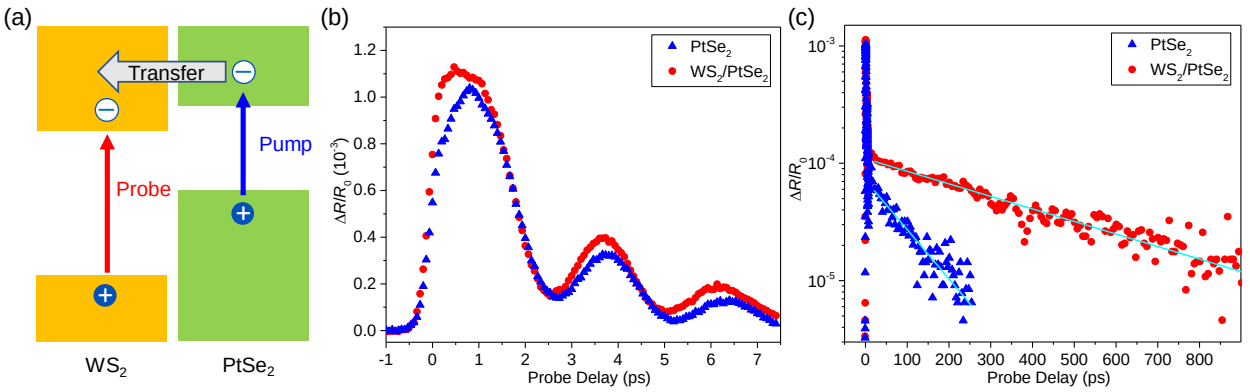

Figure 4: (a) Schematics of the pump-probe configuration to study electron transfer from $PtSe_2$ bilayer to WS_2 monolayer. A 1.51-eV pump pulse excites carriers in $PtSe_2$ while a 2.01-eV probe pulse senses the electrons that transferred to WS_2. (b) and (c) Differential reflectance measured from the bilayer $PtSe_2$ (blue) and the heterostructure (red). The cyan curves in (c) are fits (see text).

subsequently transferred to WS_2. The measured differential reflectance signal is shown as the red circles in Figure 4(b) and 4(c), along with the result of the same measurement performed on bilayer $PtSe_2$ (blue triangles). The oscillatory feature observed in the few-ps range from bilayer $PtSe_2$ is due to coherent lattice vibration, with the period and decay time being both consistent with previous results.[59,60] After this short-lived feature, the carrier-induced signal decays exponentially with a decay constant of 103 ± 5 ps (cyan curve over the blue triangles), which is consistent with recent results on carrier dynamics in 2D $PtSe_2$.[25,61–63] The signal from the heterostructure shows similar oscillatory feature in early probe delays. However, the rest of the signal decays much slower, with a decay constant of 403 ± 10 ps. If the electron transfer from $PtSe_2$ to WS_2 is absent, the two signals should be similar, since both would reflect the dynamics in the bilayer $PtSe_2$. The observed long-lived signal can thus be attributed to the interlayer excitons formed between the transferred electrons the holes that reside in $PtSe_2$. Due to the strong oscillatory feature in early probe delays, we cannot directly probe the transfer time of these electrons. However, both the results shown in Figure 2 and the significant long-lived component of the signal observed here suggest that the CT occurs on an ultrafast time scale. Furthermore, when the same measurement is performed on monolayer WS_2, no signal is observed (see Supporting Information Figure

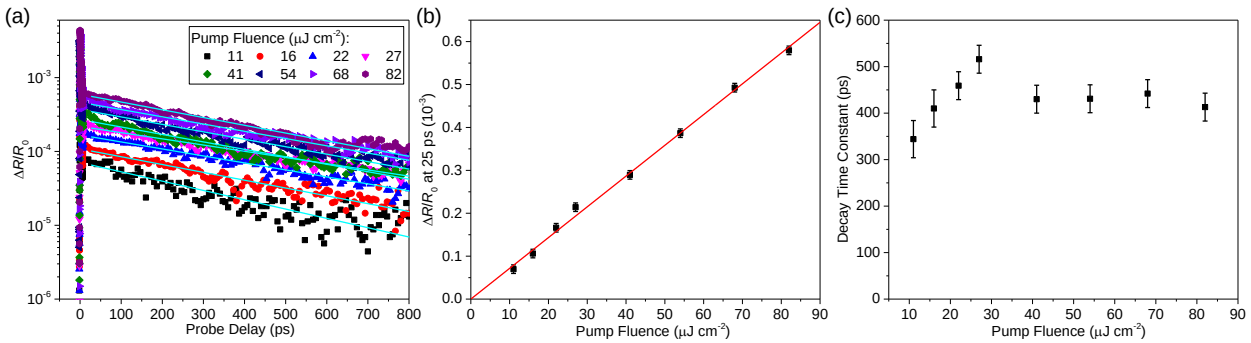

Figure 5: (a) Differential reflectance measured from the $WS_2/PtSe_2$ heterostructure sample with the configuration shown in Figure 4(a) but with various pump fluences. (b) The signal at 25 ps versus the pump fluence. (c) Decay time constant versus the pump fluence deduced from exponential fits shown as the cyan curves in (a).

S2). This confirms that WS_2 is not excited and thus the electrons observed are transferred from $PtSe_2$.

Next, the measurement is repeated with different fluences of the 1.51-eV pump, as shown in Figure 5(a). The signal at 25 ps (that is, after the oscillatory part) is proportional to the pump fluence [Figure 5(b)]. Hence, the signal decay directly reflects that of the carrier density. By single exponential fits [cyan curves in Figure 5(a)], the decay time constant at each pump fluence is deduced and summarized in Figure 5(c), which is nearly independent of the pump fluence. This shows that the interlayer exciton lifetime is density-independent in this range.

The in-plane diffusion of the interlayer excitons is studied by spatially resolved measurements. Here, the focused 3.02-eV pump pulse injects photocarriers in both layers. After the CT process, interlayer excitons with a Gaussian spatial distribution are formed with the electrons and holes in the WS_2 and $PtSe_2$ layers, respectively. Figure 6(a) shows the differential reflectance of the 2.01-eV probe versus the probe delay and probe position. A few spatially profiles are shown in Figure 6(b). The squared width deduced from such fits is plotted in Figure 6(c) against the probe delay. For a classical diffusion process with a diffusion coefficient D and an initial exciton density profile width W_0, the full width at half maximum width of the profile evolves as $w^2(t) = w_0^2 + 11.09Dt$.[52,64,65] A linear fit (the red

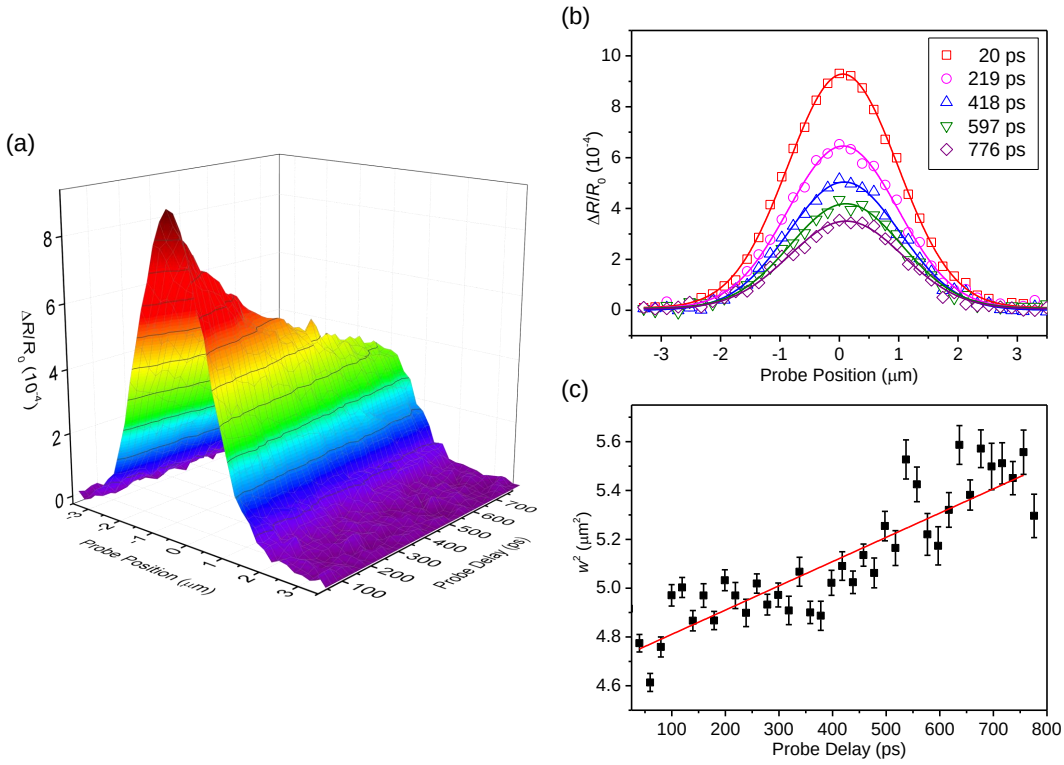

Figure 6: (a) Differential reflectance as a function of the probe delay and probe position measured from the $WS_2/PtSe_2$ heterostructure sample with 3.02-eV pump and 2.01-eV probe pulse. (b) Examples of the spatial profiles of the signal at various probe delays. The curves are Gaussian fits to the data. (c) Squared width of the profiles as a function of the probe delay. The red line is a linear fit to the data.

line) yields $D = 0.9 \pm 0.2$ cm^2 s^{-1}. This value is significantly smaller than the intralayer exciton diffusion coefficient of monolayer WS_2.[66–68] However, owing to their long lifetime (τ) of about 400 ps, the diffusion length of these interlayer excitons reaches $\sqrt{D\tau} = 200$ nm.

Conclusions

In summary, photoluminescence spectroscopy and layer-selective transient absorption measurements with various pump-probe configurations showed ultrafast interlayer CT in the heterostructure formed by bilayer $PtSe_2$ and monolayer WS_2, confirming its type-II band alignment with the CBM and VBM located in WS_2 and $PtSe_2$ layers, respectively. The CT facilitates formation of the interlayer excitons with a lifetime of several hundred ps to 1 ns, a

diffusion coefficient of 0.9 cm^2 s^{-1}, and a diffusion length of 200 nm. In this study, all measurements are performed with the sample under ambient condition and at room temperature. However, a recent study has revealed that the ultrafast interlayer CT is rather robust against lattice temperature.[69] Our results demonstrate integration of $PtSe_2$ with other 2D materials with novel CT properties and help develop fundamental understanding on the performance of various optoelectronic devices based on 2D heterostructures involving $PtSe_2$.

Experimental Method

Sample Fabrication. The bilayer $PtSe_2$ films are prepared by 6 Carbon Technology Corporation by chemical vapor deposition on c-cut sapphire substrates. To obtain WS_2 monolayers, a bulk WS_2 crystal from 2D Semiconductors is first exfoliated by an adhesive tape. The produced flakes are transferred to a polydimethylsiloxane substrate by press the take against it, followed by quickly peeling of the tape. The flakes reside on the polydimethylsiloxane substrate are examined under an optical microscope to identity monolayer flakes according to their optical contrast. A selected monolayer WS_2 flake is transferred onto a bilayer $PtSe_2$ film by first overlaying the two substrates and then lowering the former onto the latter, followed by quick lifting-up. Another monolayer WS_2 flake is transferred onto the same substrate that is not covered by $PtSe_2$.

Transient Absorption Measurements. The transient absorption measurements are done in the reflection geometry. The laser system is based on a Newport Ti:sapphire laser with a reparation rate of 80 MHz, a temporal pulse width of 100 fs, and wavelength of 820 nm. An optical parametric oscillator with a second-harmonic-generation unit is pumped by the Ti:sapphire laser, producing pulses in the range of 500 - 750 nm. The Ti:sapphire output is also used to generate its second harmonic at 410 nm in a nonlinear optical crystal. Depending on the measurement configuration, two of these pulses are selected as pump and probe, which are combined by a beamsplitter and co-focused on the sample by an objective.

The pump is modulated by a chopper at about 3 KHz. A lock-in amplifier measures the voltage output of a photodiode that received the reflected probe. The differential reflectance ($\Delta R/R_0 = (R - R_0)/R_0$, where R and R_0 are the probe reflectance with and without the pump, respectively), is recorded as a function of the probe delay to reveal the carrier dynamics.

Supporting Information Available

The Supporting Information is available free of charge at https://pubs.acs.org.

Transient absorption signal from monolayer WS_2 with 3.02-eV pump and 2.01-eV probe pulses and with various pump fluences, transient absorption signal from monolayer WS_2 with 1.51-eV pump and 2.01-eV probe pulses.

ACKNOWLEDGMENTS

Y.W. and D.H. are grateful to acknowledge the finical support from National Natural Science Foundation of China (Grant No.: 61875236, 61905010, 61975007) and Beijing Natural Science Foundation of China (Grant No.: Z190006). J.H. acknowledges the Fundamental Research Funds for the Central Universities (buctrc202003). X.Z. acknowledges the financial support from National Nature Science Foundation of China (Grant No.: 11974088). H.Z. is supported by the U.S. Department of Energy, Office of Basic Energy Sciences, Division of Materials Sciences and Engineering under Award DE-SC0020995.

References

(1) Oyedele, A. D.; Yang, S. Z.; Liang, L. B.; Puretzky, A. A.; Wang, K.; Zheng, J. J.; Yu, P.; Pudasaini, P. R.; Ghosh, A. W.; Liu, Z.; Rouleau, C. M.; Sumpter, B. G.; Chisholm, M. F.; Zhou, W.; Rack, P. D.; Geohegan, D. B.; Xiao, K. $PdSe_2$: Pentagonal

Two-Dimensional Layers with High Air Stability for Electronics. *J. Am. Chem. Soc.* **2017**, *139*, 14090–14097.

(2) Wang, G. Z.; Wang, Z. Z.; McEvoy, N.; Fan, P.; Blau, W. J. Layered $PtSe_2$ for Sensing, Photonic, and (Opto-)Electronic Applications. *Adv. Mater.* **2021**, *33*, 2004070.

(3) Lin, X.; Lu, J. C.; Shao, Y.; Zhang, Y. Y.; Wu, X.; Pan, J. B.; Gao, L.; Zhu, S. Y.; Qian, K.; Zhang, Y. F.; Bao, D. L.; Li, L. F.; Wang, Y. Q.; Liu, Z. L.; Sun, J. T.; Lei, T.; Liu, C.; Wang, J. O.; Ibrahim, K.; Leonard, D. N.; Zhou, W.; Guo, H. M.; Wang, Y. L.; Du, S. X.; Pantelides, S. T.; Gao, H. J. Intrinsically Patterned Two-Dimensional Materials for Selective Adsorption of Molecules and Nanoclusters. *Nat. Mater.* **2017**, *16*, 717–722.

(4) Wang, Z. G.; Li, Q.; Besenbacher, F.; Dong, M. D. Facile Synthesis of Single Crystal $PtSe_2$ Nanosheets for Nanoscale Electronics. *Adv. Mater.* **2016**, *28*, 10224–10229.

(5) O'Brien, M.; McEvoy, N.; Motta, C.; Zheng, J. Y.; Berner, N. C.; Kotakoski, J.; Elibol, K.; Pennycook, T. J.; Meyer, J. C.; Yim, C.; Abid, M.; Hallam, T.; Donegan, J. F.; Sanvito, S.; Duesberg, G. S. Raman Characterization of Platinum Diselenide Thin Films. *2D Mater.* **2016**, *3*, 021004.

(6) Wu, D.; Guo, J. W.; Du, J.; Xia, C. X.; Zeng, L. H.; Tian, Y. Z.; Shi, Z. F.; Tian, Y. T.; Li, X. J.; Tsang, Y. H.; Jie, J. S. Highly Polarization-Sensitive, Broadband, Self-Powered Photodetector Based on Graphene/$PdSe_2$/Germanium Heterojunction. *ACS Nano* **2019**, *13*, 9907–9917.

(7) Zhao, Y. D.; Qiao, J. S.; Yu, P.; Hu, Z. X.; Lin, Z. Y.; Lau, S. P.; Liu, Z.; Ji, W.; Chai, Y. Extraordinarily Strong Interlayer Interaction in 2D Layered PtS_2. *Adv. Mater.* **2016**, *28*, 2399–2407.

(8) Chia, X. Y.; Adriano, A.; Lazar, P.; Sofer, Z.; Luxa, J.; Pumera, M. Layered Platinum

Dichalcogenides (PtS_2, $PtSe_2$, and $PtTe_2$) Electrocatalysis: Monotonic Dependence on the Chalcogen Size. *Adv. Funct. Mater.* **2016**, *26*, 4306–4318.

(9) Wang, Y. L.; Li, L. F.; Yao, W.; Song, S. R.; Sun, J. T.; Pan, J. B.; Ren, X.; Li, C.; Okunishi, E.; Wang, Y. Q.; Wang, E. Y.; Shao, Y.; Zhang, Y. Y.; Yang, H. T.; Schwier, E. F.; Iwasawa, H.; Shimada, K.; Taniguchi, M.; Cheng, Z. H.; Zhou, S. Y.; Du, S. X.; Pennycook, S. J.; Pantelides, S. T.; Gao, H. J. Monolayer $PtSe_2$, a New Semiconducting Transition-Metal-Dichalcogenide, Epitaxially Grown by Direct Selenization of Pt. *Nano Lett.* **2015**, *15*, 4013–4018.

(10) Zhao, Y. D.; Qiao, J. S.; Yu, Z. H.; Yu, P.; Xu, K.; Lau, S. P.; Zhou, W.; Liu, Z.; Wang, X. R.; Ji, W.; Chai, Y. High-Electron- Mobility and Air-Stable 2D Layered $PtSe_2$ FETs. *Adv. Mater.* **2017**, *29*, 1604230.

(11) Ciarrocchi, A.; Avsar, A.; Ovchinnikov, D.; Kis, A. Thickness-Modulated Metal-to-Semiconductor Transformation in a Transition Metal Dichalcogenide. *Nat. Commun.* **2018**, *9*, 919.

(12) Yim, C.; Lee, K.; McEvoy, N.; O'Brien, M.; Riazimehr, S.; Berner, N. C.; Cullen, C. P.; Kotakoski, J.; Meyer, J. C.; Lemme, M. C.; Duesberg, G. S. High-Performance Hybrid Electronic Devices from Layered $PtSe_2$ Films Grown at Low Temperature. *ACS Nano* **2016**, *10*, 9550–9558.

(13) Shi, J. P.; Huan, Y. H.; Hong, M.; Xu, R. Z.; Yang, P. F.; Zhang, Z. P.; Zou, X. L.; Zhang, Y. F. Chemical Vapor Deposition Grown Large-Scale Atomically Thin Platinum Diselenide with Semimetal-Semiconductor Transition. *ACS Nano* **2019**, *13*, 8442–8451.

(14) Yan, M. Z.; Wang, E. Y.; Zhou, X.; Zhang, G. Q.; Zhang, H. Y.; Zhang, K. N.; Yao, W.; Lu, N. P.; Yang, S. Z.; Wu, S. L.; Yoshikawa, T.; Miyamoto, K.; Okuda, T.; Wu, Y.; Yu, P.; Duan, W. H.; Zhou, S. Y. High Quality Atomically Thin $PtSe_2$ Films Grown by Molecular Beam Epitaxy. *2D Mater.* **2017**, *4*, 045015.

(15) Yao, W.; Wang, E. Y.; Huang, H. Q.; Deng, K.; Yan, M. Z.; Zhang, K. N.; Miyamoto, K.; Okuda, T.; Li, L. F.; Wang, Y. L.; Gao, H. J.; Liu, C. X.; Duan, W. H.; Zhou, S. Y. Direct Observation of Spin-Layer Locking by Local Rashba Effect in Monolayer Semiconducting $PtSe_2$ Film. *Nat. Commun.* **2017**, *8*, 14216.

(16) Yu, X. C.; Yu, P.; Wu, D.; Singh, B.; Zeng, Q. S.; Lin, H.; Zhou, W.; Lin, J. H.; Suenaga, K.; Liu, Z.; Wang, Q. J. Atomically Thin Noble Metal Dichalcogenide: A Broadband Mid-Infrared Semiconductor. *Nat. Commun.* **2018**, *9*, 1545.

(17) Sattar, S.; Schwingenschlogl, U. Electronic Properties of Graphene-$PtSe_2$ Contacts. *ACS Appl. Mater. Interfaces* **2017**, *9*, 15809–15813.

(18) Liang, Q. J.; Wang, Q. X.; Zhang, Q.; Wei, J. X.; Lim, S. X. D.; Zhu, R.; Hu, J. X.; Wei, W.; Lee, C.; Sow, C.; Zhang, W. J.; Wee, A. T. S. High-Performance, Room Temperature, Ultra-Broadband Photodetectors Based on Air-Stable $PdSe_2$. *Adv. Mater.* **2019**, *31*, 1807609.

(19) Xu, H.; Zhang, H. M.; Liu, Y. W.; Zhang, S. M.; Sun, Y. Y.; Guo, Z. X.; Sheng, Y. C.; Wang, X. D.; Luo, C.; Wu, X.; Wang, J. L.; Hu, W. D.; Xu, Z. H.; Sun, Q. Q.; Zhou, P.; Shi, J.; Sun, Z. Z.; Zhang, D. W.; Bao, W. Z. Controlled Doping of Wafer-Scale $PtSe_2$ Films for Device Application. *Adv. Funct. Mater.* **2019**, *29*, 1805614.

(20) Avsar, A.; Ciarrocchi, A.; Pizzochero, M.; Unuchek, D.; Yazyev, O. V.; Kis, A. Defect Induced, Layer-Modulated Magnetism in Ultrathin Metallic $PtSe_2$. *Nat. Nanotechnol.* **2019**, *14*, 674–678.

(21) Luo, L. B.; Wang, D.; Xie, C.; Hu, J. G.; Zhao, X. Y.; Liang, F. X. $PdSe_2$ Multilayer on Germanium Nanocones Array with Light Trapping Effect for Sensitive Infrared Photodetector and Image Sensing Application. *Adv. Funct. Mater.* **2019**, *29*, 1900849.

(22) Geim, A. K.; Grigorieva, I. V. Van der Waals Heterostructures. *Nature* **2013**, *499*, 419–425.

(23) Fu, J. T.; Hong, M.; Shi, J. P.; Xie, C. Y.; Jiang, S. L.; Shang, Q. Y.; Zhang, Q. H.; Shi, Y. P.; Huan, Y. H.; Zhang, Z. Q.; Yang, P. F.; Li, X.; Gu, L.; Zhang, Q.; Shan, C. X.; Zhang, Y. F. Intercalation-Mediated Synthesis and Interfacial Coupling Effect Exploration of Unconventional Graphene/$PtSe_2$ Vertical Heterostructures. *ACS Appl. Mater. Interfaces* **2019**, *11*, 48221–48229.

(24) Wang, W. J.; Li, K. L.; Wang, Y.; Jiang, W. X.; Liu, X. Y.; Qi, H. Investigation of the Band Alignment at MoS_2/$PtSe_2$ Heterojunctions. *Appl. Phys. Lett.* **2019**, *114*, 201601.

(25) Zhou, J. D.; Kong, X. H.; Sekhar, M. C.; Lin, J. H.; Goualher, F. L.; Xu, R.; Wang, X. W.; Chen, Y.; Zhou, Y.; Zhu, C.; Lu, W.; Liu, F. C.; Tang, B. J.; Guo, Z. L.; Zhu, C.; Cheng, Z. H.; Yu, T.; Suenaga, K.; Sun, D.; Ji, W.; Liu, Z. Epitaxial Synthesis of Monolayer $PtSe_2$ Single Crystal on $MoSe_2$ with Strong Interlayer Coupling. *ACS Nano* **2019**, *13*, 10929–10938.

(26) Yuan, J.; Sun, T.; Hu, Z. X.; Yu, W. Z.; Ma, W. L.; Zhang, K.; Sun, B. Q.; Lau, S. P.; Bao, Q. L.; Lin, S. H.; Li, S. J. Wafer-Scale Fabrication of Two-Dimensional PtS_2/$PtSe_2$ Heterojunctions for Efficient and Broad Band Photodetection. *ACS Appl. Mater. Interfaces* **2018**, *10*, 40614–40622.

(27) Hong, X.; Kim, J.; Shi, S. F.; Zhang, Y.; Jin, C.; Sun, Y.; Tongay, S.; Wu, J.; Zhang, Y.; Wang, F. Ultrafast Charge Transfer in Atomically Thin MoS_2/WS_2 Heterostructures. *Nat. Nanotechnol.* **2014**, *9*, 682–686.

(28) Ceballos, F.; Bellus, M. Z.; Chiu, H. Y.; Zhao, H. Ultrafast Charge Separation and Indirect Exciton Formation in a MoS_2-$MoSe_2$ van der Waals Heterostructure. *ACS Nano* **2014**, *8*, 12717–12724.

(29) Gong, Y.; Lin, J.; Wang, X.; Shi, G.; Lei, S.; Lin, Z.; Zou, X.; Ye, G.; Vajtai, R.; Yakobson, B. I.; Terrones, H.; Terrones, M.; Tay, B. K.; Lou, J.; Pantelides, S. T.; Liu, Z.;

Zhou, W.; Ajayan, P. M. Vertical and In-Plane Heterostructures from WS_2/MoS_2 Monolayers. *Nat. Mater.* **2014**, *13*, 1135–1142.

(30) Lee, C. H.; Lee, G. H.; van der Zande, A. M.; Chen, W.; Li, Y.; Han, M.; Cui, X.; Arefe, G.; Nuckolls, C.; Heinz, T. F.; Guo, J.; Hone, J.; Kim, P. Atomically Thin P-N Junctions with van der Waals Heterointerfaces. *Nat. Nanotechnol.* **2014**, *9*, 676–681.

(31) Yao, P.; He, D.; Zereshki, P.; Wang, Y.; Zhao, H. Nonlinear optical effect of interlayer charge transfer in a van der Waals heterostructure. *Appl. Phys. Lett.* **2020**, *115*, 263103.

(32) Li, Y. Y.; Zhang, L.; Chang, J. H.; Cui, A. N.; Zhao, H. Time-Resolved Observation of Hole Tunneling in van der Waals Multilayer Heterostructures. *ACS Appl. Mater. Interfaces* **2021**, *13*, 12425–12431.

(33) Zheng, T.; Valencia-Acuna, P.; Zereshki, P.; Beech, K. M.; Deng, L.; Ni, Z.; Zhao, H. Thickness-Dependent Interlayer Charge Transfer in $MoSe_2/MoS_2$ Heterostructures Studied by Femtosecond Transient Absorption Measurements. *ACS Appl. Mater. Interfaces* **2021**, *13*, 6489–6495.

(34) Haigh, S. J.; Gholinia, A.; Jalil, R.; Romani, S.; Britnell, L.; Elias, D. C.; Novoselov, K. S.; Ponomarenko, L. A.; Geim, A. K.; Gorbachev, R. Cross-Sectional Imaging of Individual Layers and Buried Interfaces of Graphene-Based Heterostructures and Superlattices. *Nat. Mater.* **2012**, *11*, 764–767.

(35) Purdie, D. G.; Pugno, N. M.; Taniguchi, T.; Watanabe, K.; Ferrari, A. C.; Lombardo, A. Cleaning Interfaces in Layered Materials Heterostructures. *Nat. Commun.* **2018**, *9*, 5387.

(36) Szydlowska, B. M.; Hartwig, O.; Tywoniuk, B.; Hartman, T.; Stimpel-Lindner, T.; Sofer, Z.; McEvoy, N.; Duesberg, G. S.; Backes, C. Spectroscopic Thickness and Quality Metrics for $PtSe_2$ Layers Produced by Top-Down and Bottom-up Techniques. *2D Mater.* **2020**, *7*, 045027.

(37) Gutierrez, H. R.; Perea-Lopez, N.; Elias, A. L.; Berkdemir, A.; Wang, B.; Lv, R.; Lopez-Urias, F.; Crespi, V. H.; Terrones, H.; Terrones, M. Extraordinary room-temperature photoluminescence in triangular WS_2 monolayers. *Nano Lett.* **2013**, *13*, 3447.

(38) Mitioglu, A. A.; Plochocka, P.; Deligeorgis, G.; Anghel, S.; Kulyuk, L.; Maude, D. K. Second-order resonant Raman scattering in single-layer tungsten disulfide WS_2. *Phys. Rev. B* **2014**, *89*, 245442.

(39) Keyshar, K.; Berg, M.; Zhang, X.; Vajtai, R.; Gupta, G.; Chan, C. K.; Beechem, T. E.; Ajayan, P. M.; Mohite, A. D.; Ohta, T. Experimental Determination of the Ionization Energies of $MoSe_2$, WS_2, and MoS_2 on SiO_2 Using Photoemission Electron Microscopy. *ACS Nano* **2017**, *11*, 8223–8230.

(40) Guo, Y. Z.; Robertson, J. Band Engineering in Transition Metal Dichalcogenides: Stacked *Versus* Lateral Heterostructures. *Appl. Phys. Lett.* **2016**, *108*, 233104.

(41) Gong, C.; Zhang, H. J.; Wang, W. H.; Colombo, L.; Wallace, R. M.; Cho, K. J. Band Alignment of Two-Dimensional Transition Metal Dichalcogenides: Application in Tunnel Field Effect Transistors. *Appl. Phys. Lett.* **2013**, *103*, 053513.

(42) Kang, J.; Tongay, S.; Zhou, J.; Li, J. B.; Wu, J. Q. Band Offsets and Heterostructures of Two-Dimensional Semiconductors. *Appl. Phys. Lett.* **2013**, *102*, 012111.

(43) Komsa, H. P.; Krasheninnikov, A. V. Electronic Structures and Optical Properties of Realistic Transition Metal Dichalcogenide Heterostructures from First Principles. *Phys. Rev. B* **2013**, *88*, 085318.

(44) Özcelik, V. O.; Azadani, J. G.; Yang, C.; Koester, S. J.; Low, T. Band Alignment of Two-Dimensional Semiconductors for Designing Heterostructures with Momentum Space Matching. *Phys. Rev. B* **2016**, *94*, 035125.

(45) Li, P. F.; Li, L.; Zeng, X. C. Tuning the Electronic Properties of Monolayer and Bilayer $PtSe_2$ *via* Strain Engineering. *J. Mater. Chem. C* **2016**, *4*, 3106–3112.

(46) Chung, C. C.; Yeh, H.; Wu, P. H.; Lin, C. C.; Li, C. S.; Yeh, T. T.; Chou, Y.; Wei, C. Y.; Wen, C. Y.; Chou, Y. C.; Luo, C. W.; Wu, C. I.; Li, M. Y.; Li, L. J.; Chang, W. H.; Chen, C. W. Atomic-Layer Controlled Interfacial Band Engineering at Two-Dimensional Layered $PtSe_2$/Si Heterojunctions for Efficient Photoelectrochemical Hydrogen Production. *ACS Nano* **2021**, *15*, 4627–4635.

(47) Jin, C. H.; Ma, E. Y.; Karni, O.; Regan, E. C.; Wang, F.; Heinz, T. F. Ultrafast Dynamics in van der Waals Heterostructures. *Nat. Nanotechnol.* **2018**, *13*, 994–1003.

(48) Raja, A.; Chaves, A.; Yu, J.; Arefe, G.; Hill, H. M.; Rigosi, A. F.; Berkelbach, T. C.; Nagler, P.; Schuller, C.; Korn, T.; Nuckolls, C.; Hone, J.; Brus, L. E.; Heinz, T. F.; Reichman, D. R.; Chernikov, A. Coulomb Engineering of the Bandgap and Excitons in Two-Dimensional Materials. *Nat. Commun.* **2017**, *8*, 15251.

(49) Hao, S.; Bellus, M. Z.; Wang, D. H. Y.; Zhao, H. Controlling exciton transport in monolayer $MoSe_2$ by dielectric screening. *Nanoscale Horiz.* **2020**, *5*, 139–143.

(50) Zheng, T.; Lin, Y.-C.; Yu, Y. L.; Valencia-Acuna, P.; Puretzky, A. A.; Torsi, R.; Liu, C. Z.; Ivanov, I. N.; Duscher, G.; Geohegan, D. B.; Ni, Z. H.; Xiao, K.; Zhao, H. Excitonic Dynamics in Janus MoSSe and WSSe Monolayers. *Nano Lett.* **2021**, *21*, 931–937.

(51) Xie, J. F.; Zhang, D.; Yan, X. Q.; Ren, M. X.; Zhao, X.; Liu, F.; Sun, R. X.; Li, X. K.; Li, Z.; Chen, S. Q.; Liu, Z. B.; Tian, J. G. Optical Properties of Chemical Vapor Deposition-Grown $PtSe_2$ Characterized by Spectroscopic Ellipsometry. *2D Mater.* **2019**, *6*, 035011.

(52) Ceballos, F.; Zhao, H. Ultrafast Laser Spectroscopy of Two-Dimensional Materials beyond Graphene. *Adv. Funct. Mater.* **2017**, *27*, 1604509.

(53) Ceballos, F.; Cui, Q.; Bellus, M. Z.; Zhao, H. Exciton Formation in Monolayer Transition Metal Dichalcogenides. *Nanoscale* **2016**, *8*, 11681–11688.

(54) Steinleitner, P.; Merkl, P.; Nagler, P.; Mornhinweg, J.; Schuller, C.; Korn, T.; Chernikov, A.; Huber, R. Direct Observation of Ultrafast Exciton Formation in a Monolayer of WSe_2. *Nano Lett.* **2017**, *17*, 1455–1460.

(55) Valencia-Acuna, P.; Zereshki, P.; Tavakoli, M. M.; Park, J.-H.; Kong, J.; Zhao, H. Transient Absorption of Transition Metal Dichalcogenide Monolayers Studied by a Photodope-Pump-Probe Technique. *Phys. Rev. B* **2020**, *102*, 035414.

(56) Boyd, R. W. *Nonlinear Optics*, 3rd ed.; Academy Press: San Diego, USA, 2008.

(57) Kumar, N.; Cui, Q.; Ceballos, F.; He, D.; Wang, Y.; Zhao, H. Exciton-Exciton Annihilation in $MoSe_2$ Monolayers. *Phys. Rev. B* **2014**, *89*, 125427.

(58) Sun, D.; Rao, Y.; Reider, G. A.; Chen, G.; You, Y.; Brezin, L.; Harutyunyan, A. R.; Heinz, T. F. Observation of Rapid Exciton-Exciton Annihilation in Monolayer Molybdenum Disulfide. *Nano Lett.* **2014**, *14*, 5625–5629.

(59) Chen, X.; Zhang, S. F.; Wang, L.; Huang, Y. F.; Liu, H. Y.; Huang, J. W.; Dong, N. N.; Liu, W. M.; Kislyakov, I. M.; Nunzi, J. M.; Zhang, L.; Wang, J. Direct Observation of Interlayer Coherent Acoustic Phonon Dynamics in Bilayer and Few-Layer $PtSe_2$. *Photo. Res.* **2019**, *7*, 1416–1424.

(60) Qiu, W. T.; Liang, W. Z.; Guo, J.; Fang, L. M.; Li, N.; Feng, Q. G.; Luo, S. N. Thickness-Dependent Ultrafast Hot Carrier and Phonon Dynamics of $PtSe_2$ Films Measured with Femtosecond Transient Optical Spectroscopy. *J. Phys. D* **2021**, *54*, 075102.

(61) Wang, G. Z.; Wang, K. P.; McEvoy, N.; Bai, Z. Y.; Cullen, C. P.; Murphy, C. N.; McManus, J. B.; Mogan, J. J.; Smith, C. M.; Duesberg, G. S.; Kaminer, I.; Wang, J.;

Blau, W. J. Ultrafast Carrier Dynamics and Bandgap Renormalization in Layered $PtSe_2$. *Small* **2019**, *15*, 1902728.

(62) Wang, L.; Zhang, S. F.; McEvoy, N.; Sun, Y. Y.; Huang, J. W.; Xie, Y. F.; Dong, N. N.; Zhang, X. Y.; Kislyakov, I. M.; Nunzi, J. M.; Zhang, L.; Wang, J. Nonlinear Optical Signatures of the Transition from Semiconductor to Semimetal in $PtSe_2$. *Laser Photonics Rev.* **2019**, *13*, 1900052.

(63) Zhao, X.; Liu, F.; Liu, D. Q.; Yan, X. Q.; Huo, C. F.; Hui, W. W.; Xie, J. F.; Ye, Q.; Guo, C. C.; Yao, Y.; Liu, Z. B.; Tian, J. G. Thickness-Dependent Ultrafast Nonlinear Absorption Properties of $PtSe_2$ Films with Both Semiconducting and Semimetallic Phases. *Appl. Phys. Lett.* **2019**, *115*, 263102.

(64) Cui, Q.; Lipatov, A.; Wilt, J. S.; Bellus, M. Z.; Zeng, X. C.; Wu, J.; Sinitskii, A.; Zhao, H. Time-Resolved Measurements of Photocarrier Dynamics in TiS_3 Nanoribbons. *ACS Appl. Mater. Interfaces* **2016**, *8*, 18334–18338.

(65) Rochford, C.; Kumar, N.; Liu, J.; Zhao, H.; Wu, J. All-Optical Technique to Correlate Defect Structure and Carrier Transport in Transferred Graphene Films. *ACS Appl. Mater. Interfaces* **2013**, *5*, 7176.

(66) Fu, Y.; He, D.; He, J.; Bian, A.; Zhang, L.; Liu, S.; Wang, Y.; ; Zhao, H. Effect of Dielectric Environment on Excitonic Dynamics in Monolayer WS_2. *Adv. Mater. Interfaces* **2019**, *6*, 1901307.

(67) Kulig, M.; Zipfel, J.; Nagler, P.; Blanter, S.; Schuller, C.; Korn, T.; Paradiso, N.; Glazov, M. M.; Chernikov, A. Exciton Diffusion and Halo Effects in Monolayer Semiconductors. *Phys. Rev. Lett.* **2018**, *120*, 207401.

(68) Kang, J. W.; Jung, J. W.; Lee, T.; Kim, J. G.; Cho, C. H. Enhancing Exciton Diffusion in Monolayer WS_2 with *h*-BN Bottom Layer. *Phys. Rev. B* **2019**, *100*, 205304.

(69) Zhou, H. Z.; Zhao, Y. D.; Zhu, H. M. Dielectric Environment-Robust Ultrafast Charge Transfer between Two Atomic Layers. *J. Phys. Chem. Lett.* **2019**, *10*, 150–155.

TOC Graphic